THE JOURNAL OF PHYSICAL CHEMISTRY C

Article

pubs.acs.org/JPCC

Spin Transport of Polyacetylene Chains Bridging Zigzag Graphene Nanoribbon Electrodes: A Nonequilibrium Treatment of Structural Control and Spin Filtering

Aldilene Saraiva-Souza,*[,†,§] Manuel Smeu,*[,†] Humberto Terrones,[‡,§] Antonio Gomes Souza Filho,[§] and Mark A. Ratner[†]

[†]Department of Chemistry, Northwestern University, 2145 Sheridan Road, Evanston, Illinois, 60208-3113, United States

[‡]Department of Physics, Pennsylvania State University, University Park, Pennsylvania 16802, United States

[§]Departamento de Física, Universidade Federal do Ceará, 60455-900, Fortaleza, Ceará, Brazil

ABSTRACT: We investigate spin transport properties in a junction composed of a polyacetylene chain bridging two zigzag graphene nanoribbon (ZGNR) electrodes with antiferromagnetic (AF) and ferromagnetic (FM) ordering. The transport calculations are carried out using a nonequilibrium Green's function (NEGF) technique combined with density functional theory (DFT). Previous studies have demonstrated that the ZGNRs exhibit a special AF ordering and half-metallicity at edge states, both of which can be destroyed by applying a strong external electric field. Moreover a stable FM state can be found in ZGNRs under an electric field. Here we demonstrate that the connection between the molecular bridge and nonequivalent carbon atoms (A/B) in the graphene sublattice of ZGNRs may occur in two bonding arrangements and can produce either metallic or semiconducting systems depending on the local coupling. By considering the carbon ring where the chain is attached, one connection resembles a para-linkage in benzene while the other connection is similar to a meta-linkage. This results in different conductances for these configurations, which may be controlled by field-effect gating. Finally, the spin filter efficiency as a function of electric field for these systems, which exhibit intrinsic AF ordering coupled to FM electrodes, is discussed.

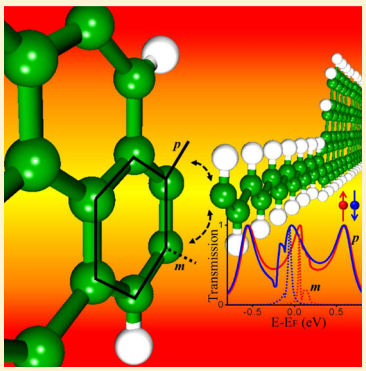

INTRODUCTION

The field of molecular electronics includes the search for novel carbon-based materials with low dimensionality, such as fullerenes, carbon nanotubes, and graphene, which may be useful as electronic components. These materials, with amazing electronic and magnetic properties, promise to minimize power consumption and to enhance operation speeds; they may be components of future electronic devices.[1−3] Graphene sheets and nanoribbons have been intensively studied because of their unique structure and strong quantum confinement effects.[4−6] In particular, the properties of graphene nanoribbons are strongly dependent on the atomic arrangement of their edges.[7] Specifically, the zigzag graphene nanoribbons (ZGNRs) have fascinating properties including magnetic states localized at the Fermi energy (E_F), where the polarized electron spin has antiferromagnetic (AF) ordering that is coupled between the two opposite edges.[8,9] The AF ordering at the edges can be controlled by an electric field applied across the ribbon and may result in spin selective control over the ZGNRs properties.[10] The ZGNRs with imperfect edges or edge modification have been shown to exhibit strong ferromagnetic (FM) behavior and have nonzero spin conductance;[11,12] these magnetic properties may potentially be applied in spin filtering systems[13−16] that might be controlled with the application of an electric field. Recent studies predict that molecular junction systems such as zigzag−armchair[17] and zigzag−zigzag[18] combinations of ZGNRs exhibit half-metallicity and conductance, strongly dependent on the nature of the molecular junction.

For single molecules attached between metal electrodes, experiment and theory have shown interference effects depending on different anchoring positions.[19] For example, if two electrodes are connected relative to one another at the para-positions on a benzene ring, the conductance through the molecule will be very different than if the connection were at meta-positions.[20] This is a manifestation of quantum interference in electron conduction.[21] A study has demonstrated that the properties of spin filtering can also depend on the linker positions (para or meta) in benzene rings.[22] The spin filtering is strong in systems that have a large spin density.[20] Finding this characteristic in molecules is less common than in ZGNRs, where the half-metallicity is a natural behavior.

Technological applications of molecular devices are still far from becoming a reality partly because fundamental issues such as the thermal stability of these devices and the nature of the metal−organic coupling are not yet completely addressed. Inconsistencies exist regarding surface charge distribution, chemical composition, and the quality of molecule−metal

Received: September 12, 2013

   dx.doi.org/10.1021/jp4091443 | J. Phys. Chem. C XXXX, XXX, XXX−XXX

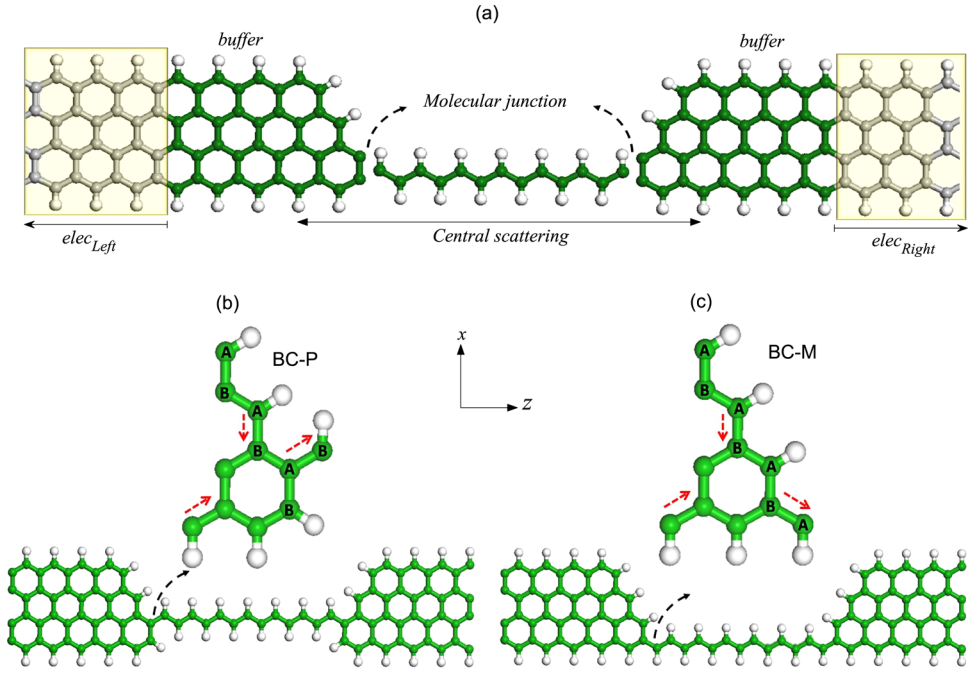

Figure 1. (a) Two-probe transport geometry. The central scattering region contains the polyacetylene bridge as well as several buffer layers of each electrode. The shaded regions include the two semi-infinite electrodes. The enlarged figures show (b) the connection of the polyacetylene bridge to ZGNR to make the BC-P (para/ortho linkages) system and (c) the connection to form the BC-M (meta linkage). A and B represent the different A/B sublattice carbon atoms.

coupling, which is responsible for charge transfer and reflection effects.[23−26] These challenges may be overcome by the use of graphene in lieu of metal electrodes, since the interface would then consist of C−C bonds. In such cases, the ZGNR structure is energetically most stable for connecting linear carbon chains with sp or sp^2 hybridization due to the extended π-system of graphene.[27,28]

In this paper, we investigate spin-polarized transport properties of the molecular junction between polyacetylene and ZGNR electrodes with AF or FM configuration using a nonequilibrium Green's function (NEGF) technique combined with density functional theory (DFT). The two-probe geometry corresponds to a central scattering region containing a molecular bridge connected to the semi-infinite ZGNR electrodes (Figure 1a). Note that the central region also includes parts of each electrode (as buffer layers), which ensures that the electronic potential and density are smooth at the boundaries with the electrodes. This arrangement of carbon atoms as electrodes has been shown to have high stability and half-metallicity,[29] and they were selected to solve an important problem of interconnection in molecular transport junctions.[30]

Since the graphene unit cell contains two nonequivalent carbon atoms that form the A and B sublattices, there are two possibilities for connecting the polyacetylene chain to the 4-ZGNRs electrodes. Several insights can be realized with these geometries. In one case the bridge can connect to the A atom of the 4-ZGNRs, resulting in a local para-linkage (BC-P system, Figure 1b), or the bridge can connect to the B atom of the 4-ZGNRs, resulting in a local meta-linkage (BC-M system, Figure 1c), as indicated by the red arrows in Figure 1. This assessment is made knowing that the current density through a ZGNR is predominantly along the edge of the ribbon (vide infra).[11] For each system, the current density can follow the bottom edge of the ZGNR and through the polyacetylene chain or it can follow the top edge and then along the end of the ZGNR and down to the polyacetylene chain. For BC-P, the polyacetylene bridge is at a para-position relative to the bottom edge of the ZGNR and at an ortho-position relative to the edge where the ribbon is terminated (see red arrows in Figure 1b). On the other hand, for BC-M, the polyacetylene bridge is in the meta-position relative to these edges, as shown by the red arrows in Figure 1c. The shape of the electrode ends was chosen as a simple model to compare para and meta attachment positions of the polyacetylene chain to the ZGNRs. We acknowledge that the shape of the electrode end would play a role in the conductance properties, but this phenomenon is beyond the scope of this work. In terms of comparing the meta/para connections, the overall structures are consistent such that meaningful comparisons can be made.

We are interested in spin transport properties that include spin density polarization in different parts of the geometry under an external electric field. Our results suggest that the BC-P system has high transmission and the BC-M system exhibits the properties of a spin filter when it is coupled to ZGNR electrodes having FM ordering. These systems might be important for applications as switches and spin valves.

■ COMPUTATIONAL DETAILS

We first focus on the electronic structure for the central scattering region system (Figure 1a), where we created periodic conditions in the (longitudinal) z-direction along the 4-ZGNRs. The periodic system is a cubic supercell containing the BC-P or BC-M systems (Figure 1b and Figure 1c). The electronic structure and geometry optimizations were performed using DFT[31,32] with the SIESTA code,[33] which provides self-consistent calculations by expanding the Kohn−Sham (KS) orbitals as a linear combination of atomic orbitals (LCAO) for the valence electrons. The norm-conserving Troullier−Martins pseudopotentials[34] were used to describe the core electrons. The valence electronic orbitals of the systems were described using a double-ζ polarized basis set.[35] Exchange-correlation is taken into account

dx.doi.org/10.1021/jp4091443 | J. Phys. Chem. C XXXX, XXX, XXX−XXX

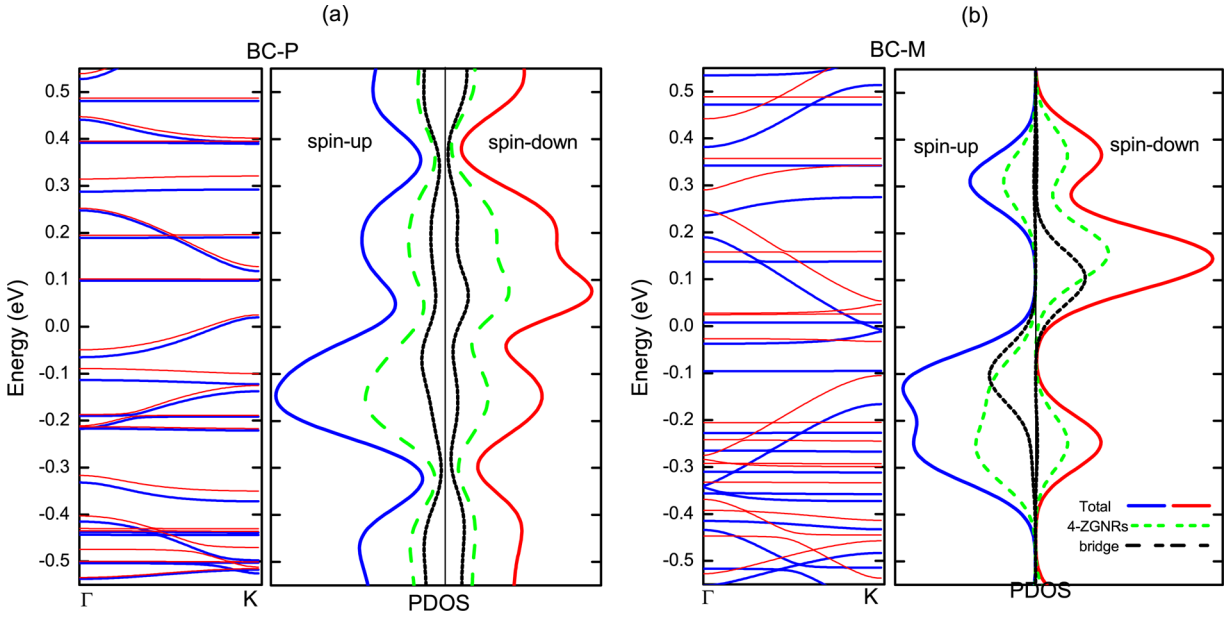

Figure 2. Electronic band structure and projected density of states (arbitrary units) for (a) BC-P and (b) BC-M systems at zero electric field. The solid dark blue lines and light red lines denote spin-up and spin-down, respectively. Note the difference in the bands around the Fermi energy ($E_F = 0$) in the BC-P and BC-M systems.

within the local spin density approximation (LSDA).[36−38] A cutoff energy of 150 Ry was used, and in all cases, the relaxed atomic configuration was obtained using a convergence force criterion of less than 0.05 eV/Å on each atom. The relaxed structures are shown in Figure 1b and Figure 1c. For both cases, the ZGNR part of the system is similar having C−C bond lengths varying as 1.43, 1.46, 1.44, and 1.45 Å going from the edge toward the middle of the ribbon (along the *x*-direction). Inside the polyacetylene chains, the C−C bond lengths were fairly uniform, being between 1.39 and 1.42 Å for the BC-P system and between 1.38 and 1.41 Å for the BC-M system.[39] The C−H bond lengths were also uniform for both systems at 1.11 or 1.12 Å.

An external electric field varying from 0.0 to 0.5 V/nm was applied across the ribbon along the positive *x*-axis (in-plane). These values keep antiferromagnetic (AF) ordering, since it has been shown that an even stronger external electric field ($\vec{E}_{ext} > 0.8$ V/nm) is needed to destroy the spin polarization and half-metallicity.[40] The Brillouin zone (BZ) was sampled as a Monkhorst−Pack grid[41] using $1 \times 1 \times 100$ *k* points.

Next, the electronic transport properties are obtained by using the TranSiesta code,[42] which employs the nonequilibrium Green's function (NEGF) technique within the Keldysh formalism in combination with DFT.[43] This technique is applied to a two-probe system, as shown in Figure 1a. Note that in our calculation all atoms are described self-consistently at the same level of theory for the central region and the electrodes. The electrodes are considered in both FM and AF configurations. The scattering states were obtained with Nanodcal, a similar NEGF-DFT code.[44,45]

This approach has been thoroughly described, and interested readers are directed to earlier articles.[44,46−51] To briefly summarize, the retarded Green's function is defined as

$$G = (E^{+}S - H - \sum_{L}(E) - \sum_{R}(E))^{-1} \quad (1)$$

where $E^{+} = \lim_{\eta \to 0} E + i\eta$ is the energy plus an infinitesimal imaginary part $i\eta$. H is the Hamiltonian, and S is the corresponding overlap matrix obtained from a conventional DFT calculation on the central scattering region. The density functional and basis set were the same as those used for the structure relaxations. $\sum_{L/R}$ are the self-energies that account for the effect of each electrode on the central scattering region. This consists of two parts; the energy level shift is given by the real part as $\Delta_{L/R}(E) = \mathrm{Re}\sum_{L/R}(E)$, and the level broadening is the imaginary part:

$$\Gamma_{L/R}(E) = i(\sum_{L/R} - \sum_{L/R}^{\dagger}) \quad (2)$$

To describe the distribution of electrons for the two-probe system, NEGF is used to calculate the density matrix of the open system within a one-particle theory such as the DFT,

$$\rho = \frac{1}{2\pi}\int_{-\infty}^{+\infty}[f(E,\mu_L)G\Gamma_L G^{\dagger} + f(E,\mu_R)G\Gamma_R G^{\dagger}]\,dE \quad (3)$$

where G is the Green's function and f is the Fermi distribution,

$$f(E,\mu) = \frac{1}{e^{(E-\mu)/(kT)} + 1} \quad (4)$$

The electrochemical potential difference between left and right electrodes is $eV = \mu_L - \mu_R$. Our focus here is on the electron transmission around the Fermi energy at zero bias $[T_\sigma(E,V{=}0)]$, where σ is the spin (up/down). The Landauer−Büttiker transmission[52] probability can be calculated as the trace over the matrix product of the coupling matrices $\Gamma_{L/R,\sigma}$[53] and the $(G/G^{\dagger})$ Green's function of the central region,

$$T_\sigma(E,V) = \mathrm{Tr}(\Gamma_{R,\sigma}G_\sigma\Gamma_{L,\sigma}G_\sigma^{\dagger}) \quad (5)$$

which represents the probability that an electron with a given energy E transmits from the left electrode, through the central region, into the right electrode. The spin filter efficiency[13,15] (SFE) at the Fermi level is defined as

$$\mathrm{SFE} = \frac{|T_{up}(E_F) - T_{down}(E_F)|}{T_{up}(E_F) + T_{down}(E_F)} \quad (6)$$

dx.doi.org/10.1021/jp4091443 | J. Phys. Chem. C XXXX, XXX, XXX−XXX

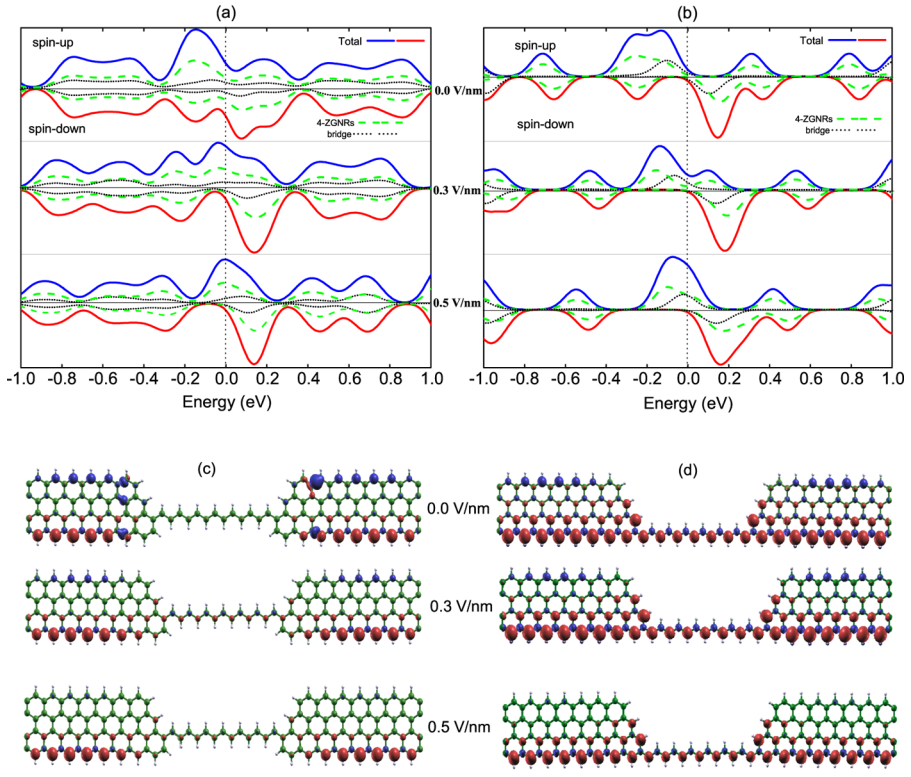

Figure 3. Projected density of states for (a) BC-P and (b) BC-M systems under different electric fields. Both systems exposed to electric field exhibit large projections around the Fermi energy. Plots of spin density isosurfaces for the (c) BC-P and (d) BC-M systems. Note that there is a magnetic moment in the bridge and that the different couplings change the ordering and the extent of the magnetization. The colors blue and red correspond to spin-up and spin-down (orbital contour value is 0.001).

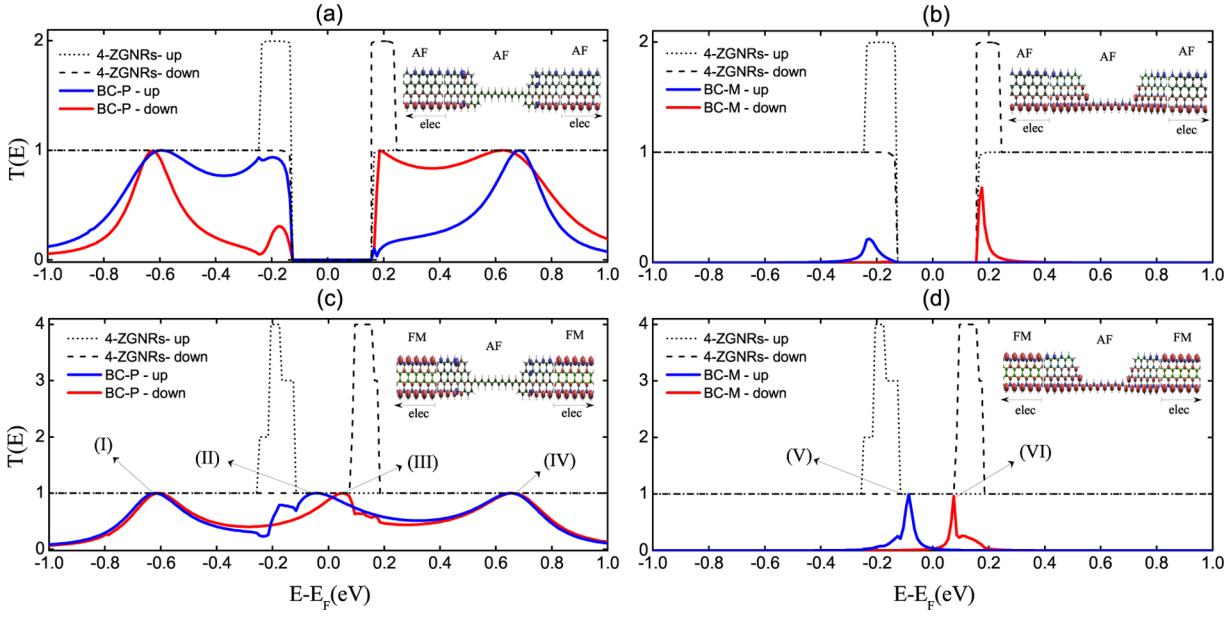

Figure 4. Transmission spectra for two-probe systems. Solid lines show spin-up/spin-down (blue/red) transmission through (a) BC-P and (b) BC-M connected to AF electrodes and (c) BC-P and (d) BC-M connected to FM electrodes. Dotted plots show transmission through perfect ZGNR for comparison.

We calculated the SFE achieved at zero bias under different electric fields for the BC-P and BC-M systems.

RESULTS

It is known that bands near the Fermi level correspond to states near the edges of the graphene nanoribbon, giving rise to the half-metallicity states. This result has been discussed extensively in the literature.[11] The interesting and relevant point here is to know how the electronic structure will be affected by the discontinuity of the 4-ZGNRs at the junctions. We first consider this by studying the electronic structure of the central region shown in Figure 1a, setting the structures shown in Figure 1b,c to

dx.doi.org/10.1021/jp4091443 | J. Phys. Chem. C XXXX, XXX, XXX−XXX

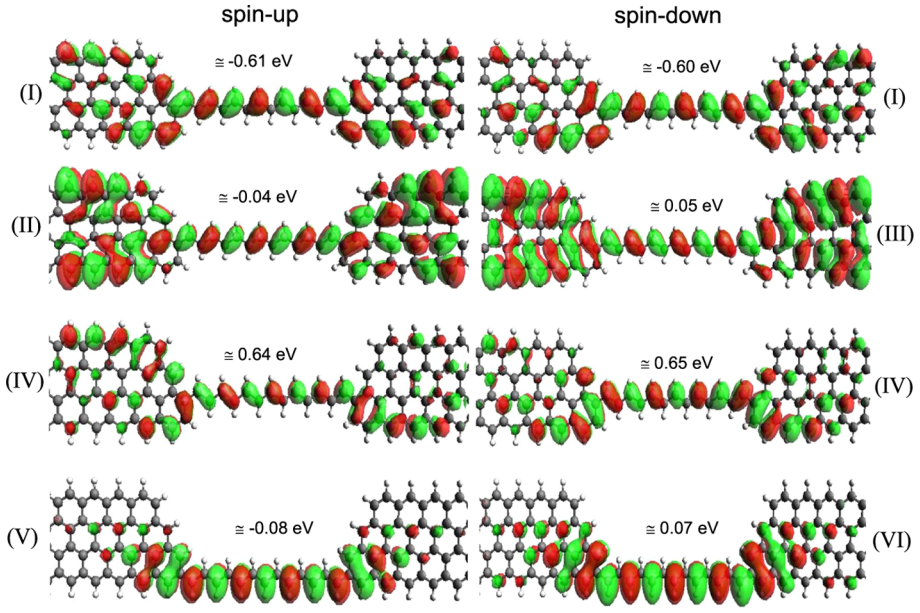

Figure 5. Scattering state wave functions for BC-P (I–IV) and BC-M (V–VI) systems. The selected energies correspond to the transmission peaks in Figure 4.

be periodic in the z-direction and calculating the band structure and the projected density of states (PDOS). In the BC-P system, an interesting behavior appears in the bands of this molecular junction (Figure 2a), especially near the Fermi energy. There is a dispersive band that clearly crosses the Fermi energy. The PDOS indicates that this dispersive level is coming from 4-ZGNRs states mixed with bridge states. Differently, in the BC-M system (Figure 2b) there is a gap in dispersive states near E_F. Overall, the relevant contribution to electron transport comes from dispersive states and whether or not they appear near the Fermi energy, an effect due to the junction between 4-ZGNRs and the bridge.

In practice, bringing a system to a regime of open conduction channels can be achieved using an electric field as a gate. The field-effect gating in the molecular junction can control the orbitals with respect to Fermi energy in two different current regimes within a large operation region, resulting in the ability to turn the current on/off. Experimental work has demonstrated a molecular field effect transistor that can be directly tuned by gate voltage.[54] In this work an external electric field ranging from 0.0 to 0.5 V/nm is applied across the systems in the x-direction. Figure 3a and Figure 3b show the PDOS of the BC-P and BC-M systems under various field strengths, projected onto the 4-ZGNRs and the polyacetylene molecular bridge. The bridge states shift in energy because of the electric field, as illustrated by the PDOS. The largest contribution comes from the 4-ZGNRs for the BC-P system, while for the BC-M system the gap around the Fermi energy shows an interesting behavior in the bridge for spin-up. The peaks near the Fermi energy are the most relevant states because they describe low-bias transport properties.

Figure 3c shows the spin density for the BC-P system under different electric fields. The spin density configurations differ slightly from 0.0 to 0.3 V/nm, with most differences being a reduction in the top half of the ZGNR and increases in the bridge. Then with a stronger field of 0.5 V/nm, the spin density is decreased in the top half while keeping the polarized states on the bridge and bottom half. The BC-M (Figure 3d) system preserves the AF ordering on the bottom side, while local magnetization is reduced on the top half which has mostly spin up configuration. In both cases the systems preserve half metallicity with different values of electric field.

Several insights can be gained from the geometry. In Figure 4, we show the transmission plots of the perfect 4-ZGNRs with electrodes having AF (a, b) and FM (c, d) configurations (dotted and dashed black lines for spin-up and spin-down, respectively). Typically, transmission peaks are very high because of edge states at zero bias. Figure 4a shows the transmission for the BC-P system coupled to AF electrodes. In this case there is a transmission gap at the E_F of about 0.27 eV for both the spin-up and spin-down, as determined by the maximum possible transmission through the perfect ZGNR. The transmission probability is similar for the two spin channels but on opposite ends of the E_F. For instance, the transmission is near unity and broad for spin-up beneath the gap at E_F while the transmission is near unity and broad for spin-down above the gap at E_F (compare solid blue and red lines in Figure 4a). In Figure 4b, we see that the transmission through the BC-M system connected to AF electrodes is much lower because of the binding geometry (meta-connection) in this system. It is interesting that the spin-down transmission peak (above E_F) is considerably larger than the spin-up transmission peak (below E_F). This is likely due to the high spin-down density along the bottom edge of the ZGNR, as shown in the inset of Figure 4b.

Figure 4c shows the transmission spectrum for the BC-P system coupled to electrodes with FM configurations, which has three broad peaks in the $[-1, 1]$ eV range. There is no gap around the Fermi energy, as was also indicated by the projected density of states (PDOS) in Figure 2a. For the BC-M system (Figure 4d), the spin-up peak localized close to the Fermi energy corresponds to a band centered near −0.1 eV (see Figure 2b). This peak is the result of a blend between 4-ZGNRs and bridge states, as we showed in Figure 3b. The spin-up and spin-down transmission spectra are quite different near the Fermi level for both structures, and in general all states are strongly influenced by the molecular junction.

dx.doi.org/10.1021/jp4091443 | J. Phys. Chem. C XXXX, XXX, XXX–XXX

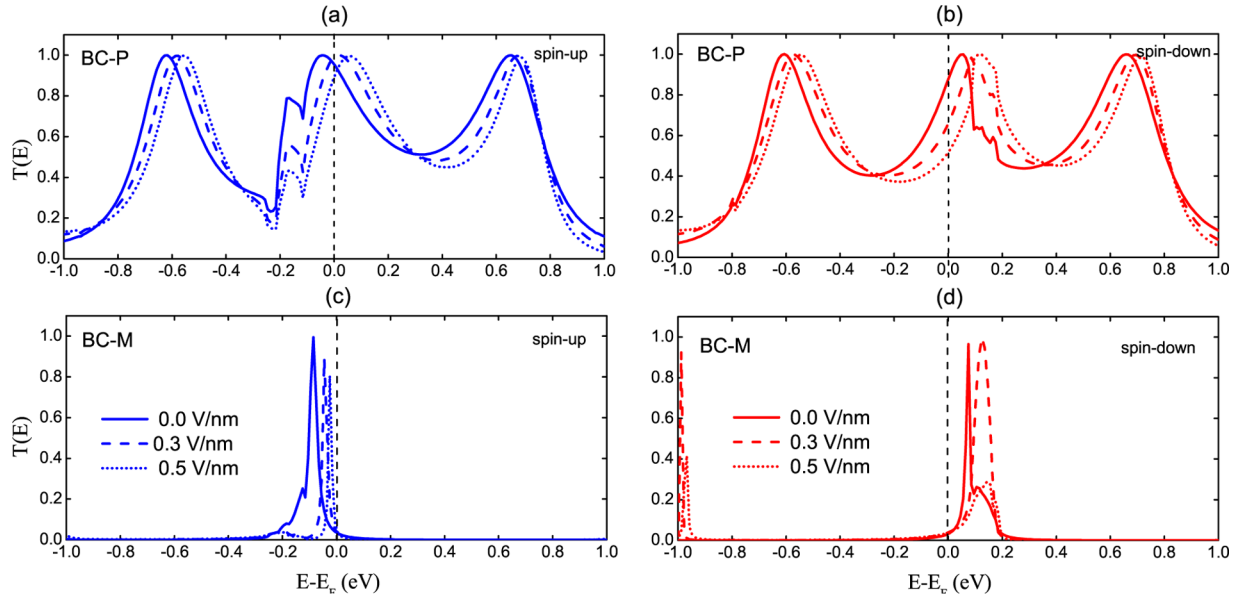

Figure 6. Spin dependent transmission spectra under external electric fields of 0.0, 0.3, and 0.5 V/nm: (a) spin-up and (b) spin-down of the BC-P system; (c) spin-up and (d) spin-down of the BC-M system.

From here on, we consider the spin configuration consisting of the FM coupling on BC-P and BC-M (AF configuration at the central region). This spin configuration is crucial for the spin filter effect.

The scattering state wave functions for different transmission peaks through BC-P and BC-M systems coupled to electrodes with FM configuration are plotted in Figure 5. They show different modes of transmission through the system for several transmission peaks in Figure 4. The isosurfaces for peaks I–IV show scattering states for the BC-P system. Note that the contributions come from the bottom edge and also the top edge of the ZGNR (para and ortho relative to polyacetylene bridge, respectively; see Figure 1b). Clearly, the contribution from peaks I–IV will result in high current. Conversely, isosurfaces V–VI for the BC-M system do not show any strong contribution from either edge of the ZGNR, since these are at meta positions relative to the polyacetylene bridge. The BC-M system shows only two narrow peaks in transmission (labeled V and VI in Figure 4). In this system, the more pronounced contribution is from the bridge as we saw in Figure 2b. These peaks are due to states localized in the bridge that extend along the center in the 4-ZGNRs.

To understand if the different transmission channels are preserved, we compare the transmission for systems under electric fields (along the *x*-axis) of 0.3 and 0.5 V/nm. Figure 6a and Figure 6b show transmission under different electric fields for the BC-P system with spin-up and spin-down, respectively. One can find transmission peaks in the same range as at 0.0 V/nm, where for spin-up there is a dip around −0.2 eV due to a ring current reversal present in the *p*-benzene system.[22,55] For this system there is a specific shift when an electric field is applied. In other words, the BC-P system preserves the resonance between different transmission channels and shows broad peaks in the same energy range for spin-up and spin-down. The BC-M system, panel c (spin-up), has a transmission peak around the Fermi energy. After application of an electric field of 0.3 and 0.5 V/nm, the width of the transmission peak decreases with increasing electric field and moves closer to E_F. Panel d shows the spin-down transmission for the same system. There is a narrow peak above E_F that is broadened and shifted away from E_F with the application of an external field of 0.3 and 0.5 V/nm.

The characteristics of spin transport shown in Figure 6, where the transmission peaks are shifted under external electric field, suggest that these systems might work as spin filters. In Table 1, we list the calculated zero-bias SFE (eq 6). For BC-P, the SFE at 0.0 V/nm is 4%, and this value increases to 21% at 0.3 V/nm and then to 25% at 0.5 V/nm. This variation in SFE suggests that the BC-P (para-linkage) system has a shift in the transmission with the help of the external electric field and may behave as a weak spin filter.

Table 1. Spin Filter Efficiency for BC-P and BC-M under Transverse Electric Fields along the *x*-Axis

electric field (V/nm)	BC-P SFE (%)	BC-M SFE (%)
0.0	4	5
0.3	21	16
0.5	25	45

The transmission spectrum of the BC-M system also showed an energy shift under the electric field, and the greatest amount of spin-filtering we found was 45%. In this case, one narrow peak (spin-up) is brought close to resonance with E_F while the other peak (spin-down) is moved away, resulting in high SFE. The strong spin filtering is due to the energy separation between the narrow spin-up and spin-down transmission peaks in this system.

SUMMARY

In this work, we used NEGF-DFT to study transport properties in ZGNR/polyacetylene molecular junctions. The two possible geometric couplings result in a local para-linkage benzene (BC-P system) or in a local meta-linkage benzene (BC-M system). We found the transmission through the BC-P system to be much higher than through the BC-M system. However, the transmission through the BC-M system can be controlled with an external electric field when it is coupled to FM electrodes. This is experimentally relevant, and to the best of our knowledge it has not been reported before for zigzag graphene nanoribbons.

dx.doi.org/10.1021/jp4091443 | J. Phys. Chem. C XXXX, XXX, XXX−XXX

Under an external electric field, we find that the BC-P system, which is metallic at zero field, remains metallic. On the other hand, for the BC-M system (semiconductor), an external electric field shifts states to the Fermi energy, and this causes the system to become conducting under a sufficient electric field. The nature of the system (weak or strong conductor) can be geometrically controlled, and the strong transmission can be explained using well-known ortho, para, and meta configuration interference rules of the benzene-like ring that is bonded to the carbon chain. Finally, we present here a proof-of-concept on how to build switches and spin filters devices based on polyacetylene chains between carbon nanoribbon electrodes.

AUTHOR INFORMATION

Corresponding Authors

*A.S.-S.: e-mail, aldi@fisica.ufc.br.

*M.S.: e-mail, manuel.smeu@northwestern.edu.

Notes

The authors declare no competing financial interest.

ACKNOWLEDGMENTS

A.S.-S. acknowledges the Brazilian agency CAPES for the Sandwich Program Fellowship (Process 1047-11-6) and CENAPA-SP for computational support. M.S. thanks the FRQNT and the NSF (Grant CHE-1058896) for financial support. M.A.R. thanks the Chemistry Division of the NSF (Grant NSF-60029645) for support. A.G.S.F. acknowledges funding from INCT NANOBIOSIMES, Fundação Cearense de Apoio ao Desenvolvimento Científico e Tecnológico (FUNCAP) through PRONEX (grant PR2-0054-00022.01.00/11) and CNPq (Grant No. 307317/2010-2). H.T. acknowledges funding from Programa Professor Visitante do Exterior (PVE) as "Bolsista CAPES/BRASIL".

REFERENCES

(1) Liu, Y.; Li, H.; Tu, D.; Ji, Z.; Wang, C.; Tang, Q.; Liu, M.; Hu, W.; Liu, Y.; Zhu, D. Controlling the Growth of Single Crystalline Nanoribbons of Copper Tetracyanoquinodimethane for the Fabrication of Devices and Device Arrays. *J. Am. Chem. Soc.* **2006**, *128*, 12917−12922.

(2) Lu, J.; Zhang, H.; Shi, W.; Wang, Z.; Zheng, Y.; Zhang, T.; Wang, N.; Tang, Z.; Sheng, P. Graphene Magnetoresistance Device in van der Pauw Geometry. *Nano Lett.* **2011**, *11*, 2973−2977.

(3) Kitaura, R.; Imazu, N.; Kobayashi, K.; Shinohara, H. Fabrication of Metal Nanowires in Carbon Nanotubes via Versatile Nano-Template Reaction. *Nano Lett.* **2008**, *8*, 693−699.

(4) Campos, L. C.; Manfrinato, V. R.; Sanchez-Yamagishi, J. D.; Kong, J.; Jarillo-Herrero, P. Anisotropic Etching and Nanoribbon Formation in Single-Layer Graphene. *Nano Lett.* **2009**, *9*, 2600−2604.

(5) Guo, B.; Liu, Q.; Chen, E.; Zhu, H.; Fang, L.; Gong, J. R. Controllable N-Doping of Graphene. *Nano Lett.* **2010**, *10*, 4975−4980.

(6) Agapito, L. A.; Kioussis, N. "Seamless" Graphene Interconnects for the Prospect of All-Carbon Spin-Polarized Field-Effect Transistors. *J. Phys. Chem. C* **2011**, *115*, 2874−2879.

(7) Nakada, K.; Fujita, M.; Dresselhaus, G.; Dresselhaus, M. S. Edge State in Graphene Ribbons: Nanometer Size Effect and Edge Shape Dependence. *Phys. Rev. B* **1996**, *54*, 17954−17961.

(8) Son, Y.-W.; Cohen, M. L.; Louie, S. G. Half-Metallic Graphene Nanoribbons. *Nature* **2006**, *444*, 347−349.

(9) Son, Y.-W.; Cohen, M. L.; Louie, S. G. Energy Gaps in Graphene Nanoribbons. *Phys. Rev. Lett.* **2006**, *97*, 216803.

(10) Rudberg, E.; Salek, P.; Luo, Y. Nonlocal Exchange Interaction Removes Half-Metallicity in Graphene Nanoribbons. *Nano Lett.* **2007**, *7*, 2211−2213.

(11) Wimmer, M.; Adagideli, I.; Berber, S.; Tománek, D.; Richter, K. Spin Currents in Rough Graphene Nanoribbons: Universal Fluctuations and Spin Injection. *Phys. Rev. Lett.* **2008**, *100*, 177207.

(12) Evaldsson, M.; Zozoulenko, I. V.; Xu, H.; Heinzel, T. Edge-Disorder-Induced Anderson Localization and Conduction Gap in Graphene Nanoribbons. *Phys. Rev. B* **2008**, *78*, 161407.

(13) Shen, X.; Sun, L.; Benassi, E.; Shen, Z.; Zhao, X.; Sanvito, S.; Hou, S. Spin Filter Effect of Manganese Phthalocyanine Contacted with Single-Walled Carbon Nanotube Electrodes. *J. Chem. Phys.* **2010**, *132*, 054703.

(14) Smeu, M.; DiLabio, G. A. Calculations of Electron Transport through Simple π- and σ-Type Radicals. *J. Phys. Chem. C* **2010**, *114*, 17874−17879.

(15) Wu, J.-C.; Wang, X.-F.; Zhou, L.; Da, H.-X.; Lim, K. H.; Yang, S.-W.; Li, Z.-Y. Manipulating Spin Transport via Vanadium−Iron Cyclopentadienyl Multidecker Sandwich Molecules. *J. Phys. Chem. C* **2009**, *113*, 7913−7916.

(16) Koleini, M.; Paulsson, M.; Brandbyge, M. Efficient Organometallic Spin Filter between Single-Wall Carbon Nanotube or Graphene Electrodes. *Phys. Rev. Lett.* **2007**, *98*, 197202.

(17) Botello-Méndez, A. R.; Cruz-Silva, E.; López-Urías, F.; Sumpter, B. G.; Meunier, V.; Terrones, M.; Terrones, H. Spin Polarized Conductance in Hybrid Graphene Nanoribbons Using 5−7 Defects. *ACS Nano* **2009**, *3*, 3606−3612.

(18) Botello-Méndez, A. R.; Cruz-Silva, E.; Romo-Herrera, J. M.; López-Urías, F.; Terrones, M.; Sumpter, B. G.; Terrones, H.; Charlier, J.-C.; Meunier, V. Quantum Transport in Graphene Nanonetworks. *Nano Lett.* **2011**, *11*, 3058−3064.

(19) Kiguchi, M.; Nakamura, H.; Takahashi, Y.; Takahashi, T.; Ohto, T. Effect of Anchoring Group Position on Formation and Conductance of a Single Disubstituted Benzene Molecule Bridging Au Electrodes: Change of Conductive Molecular Orbital and Electron Pathway. *J. Phys. Chem. C* **2010**, *114*, 22254−22261.

(20) Herrmann, C.; Solomon, G. C.; Ratner, M. A. Organic Radicals as Spin Filters. *J. Am. Chem. Soc.* **2010**, *132*, 3682−3684.

(21) Nichols, R. J.; Higgins, S. J. Molecular Junctions: Interference Comes into View. *Nat. Nanotechnol.* **2012**, *7*, 281−282.

(22) Herrmann, C.; Solomon, G. C.; Ratner, M. A. Designing Organic Spin Filters in the Coherent Tunneling Regime. *J. Chem. Phys.* **2011**, *134*, 224306.

(23) Basch, H.; Cohen, R.; Ratner, M. A. Interface Geometry and Molecular Junction Conductance: Geometric Fluctuation and Stochastic Switching. *Nano Lett.* **2005**, *5*, 1668−1675.

(24) Frei, M.; Aradhya, S. V.; Koentopp, M.; Hybertsen, M. S.; Venkataraman, L. Mechanics and Chemistry: Single Molecule Bond Rupture Forces Correlate with Molecular Backbone Structure. *Nano Lett.* **2011**, *11*, 1518−1523.

(25) Li, G.; Tamblyn, I.; Cooper, V. R.; Gao, H.-J.; Neaton, J. B. Molecular Adsorption on Metal Surfaces with van der Waals Density Functionals. *Phys. Rev. B* **2012**, *85*, 121409.

(26) Hofmann, O. T.; Egger, D. A.; Zojer, E. Work-Function Modification beyond Pinning: When Do Molecular Dipoles Count? *Nano Lett.* **2010**, *10*, 4369−4374.

(27) Jin, C.; Lan, H.; Peng, L.; Suenaga, K.; Iijima, S. Deriving Carbon Atomic Chains from Graphene. *Phys. Rev. Lett.* **2009**, *102*, 205501.

(28) Chen, W.; Andreev, A. V.; Bertsch, G. F. Conductance of a Single-Atom Carbon Chain with Graphene Leads. *Phys. Rev. B* **2009**, *80*, 085410.

(29) Chuvilin, A.; Meyer, J. C.; Algara-Siller, G.; Kaiser, U. From Graphene Constrictions to Single Carbon Chains. *New J. Phys.* **2009**, *11*, 083019.

(30) Tongay, S.; Senger, R. T.; Dag, S.; Ciraci, S. Ab-initio Electron Transport Calculations of Carbon Based String Structures. *Phys. Rev. Lett.* **2004**, *93*, 136404.

(31) Kohn, W.; Sham, L. J. Self-Consistent Equations Including Exchange and Correlation Effects. *Phys. Rev.* **1965**, *140*, A1133−A1138.

(32) Hohenberg, P.; Kohn, W. Inhomogeneous Electron Gas. *Phys. Rev.* **1964**, *136*, B864−B871.

(33) Soler, J. M.; Artacho, E.; Gale, J. D.; García, A.; Junquera, J.; Ordejón, P.; Sánchez-Portal, D. The SIESTA Method for *Ab*-Initio Order-*N* Materials Simulation. *J. Phys.: Condens. Matter* **2002**, *14*, 2745−2779.
(34) Troullier, N.; Martins, J. L. Efficient Pseudopotentials for Plane-Wave Calculations. *Phys. Rev. B* **1991**, *43*, 1993−2006.
(35) Junquera, J.; Paz, O.; Sánchez-Portal, D.; Artacho, E. Numerical Atomic Orbitals for Linear-Scaling Calculations. *Phys. Rev. B* **2001**, *64*, 235111.
(36) von Barth, U.; Hedin, L. A Local Exchange-Correlation Potential for the Spin Polarized Case. I. *J. Phys. C: Solid State Phys.* **1972**, *5*, 1629−1642.
(37) Gunnarsson, O.; Lundqvist, B. I. Exchange and Correlation in Atoms, Molecules, and Solids by the Spin-Density-Functional Formalism. *Phys. Rev. B* **1976**, *13*, 4274−4298.
(38) Rajagopal, A. K. Inhomogeneous Relativistic Electron Gas. *J. Phys. C: Solid State Phys.* **1978**, *11*, L943−L948.
(39) Note that the uniform bond lengths along the polyacetylene chain is due to the use of LSDA in this work. While the use of a nonlocal functional would have led to a geometry with greater alternation in the bond length, it has been shown that it also results in the absence of half-metallicity in ZGNRs when nonlocal exchange interaction is included.[10] Therefore, we opted to model the half-metallicity in our systems over the bond length alternation in polyacetylene.
(40) Kan, E.-J.; Li, Z.; Yang, J.; Hou, J. G. Will Zigzag Graphene Nanoribbon Turn to Half Metal Under Electric Field? *Appl. Phys. Lett.* **2007**, *91*, 243116.
(41) Monkhorst, H. J.; Pack, J. D. Special Points for Brillouin-Zone Integrations. *Phys. Rev. B* **1976**, *13*, 5188−5192.
(42) Brandbyge, M.; Mozos, J.-L.; Ordejón, P.; Taylor, J.; Stokbro, K. Density-Functional Method for Nonequilibrium Electron Transport. *Phys. Rev. B* **2002**, *65*, 165401.
(43) Datta, S. Nanoscale Device Modeling: The Green's Function Method. *Superlattices Microstruct.* **2000**, *28*, 253−278.
(44) Taylor, J.; Guo, H.; Wang, J. Ab-initio Modeling of Quantum Transport Properties of Molecular Electronic Devices. *Phys. Rev. B* **2001**, *63*, 245407.
(45) Waldron, D.; Haney, P.; Larade, B.; MacDonald, A.; Guo, H. Nonlinear Spin Current and Magnetoresistance of Molecular Tunnel Junctions. *Phys. Rev. Lett.* **2006**, *96*, 166804.
(46) Yoshizawa, K.; Tada, T.; Staykov, A. Orbital Views of the Electron Transport in Molecular Devices. *J. Am. Chem. Soc.* **2008**, *130*, 9406−9413.
(47) Deng, W.-Q.; Muller, R. P.; Goddard, W. A. Mechanism of the Stoddart−Heath Bistable Rotaxane Molecular Switch. *J. Am. Chem. Soc.* **2004**, *126*, 13562−13563.
(48) Shen, L.; Zeng, M.; Yang, S.-W.; Zhang, C.; Wang, X.; Feng, Y. Electron Transport Properties of Atomic Carbon Nanowires between Graphene Electrodes. *J. Am. Chem. Soc.* **2010**, *132*, 11481−11486.
(49) Ie, Y.; Hirose, T.; Nakamura, H.; Kiguchi, M.; Takagi, N.; Kawai, M.; Aso, Y. Nature of Electron Transport by Pyridine-Based Tripodal Anchors: Potential for Robust and Conductive Single-Molecule Junctions with Gold Electrodes. *J. Am. Chem. Soc.* **2011**, *133*, 3014−3022.
(50) Yeganeh, S.; Galperin, M.; Ratner, M. A. Switching in Molecular Transport Junctions: Polarization Response. *J. Am. Chem. Soc.* **2007**, *129*, 13313−13320.
(51) Aravena, D.; Ruiz, E. Coherent Transport through Spin-Crossover Single Molecules. *J. Am. Chem. Soc.* **2012**, *134*, 777−779.
(52) Datta, S. *Electronic Transport in Mesoscopic Systems*; Cambridge University Press: Cambridge, U.K., 1997.
(53) López Sancho, M. P.; López Sancho, J. M.; Rubio, J. Quick Iterative Scheme for the Calculation of Transfer Matrices: Application to Mo (100). *J. Phys. F: Met. Phys.* **1984**, *14*, 1205−1215.
(54) Song, H.; Kim, Y.; Jang, Y. H.; Jeong, H.; Reed, M. A.; Lee, T. Observation of Molecular Orbital Gating. *Nature* **2009**, *462*, 1039−1043.
(55) Hansen, T.; Solomon, G. C.; Andrews, D. Q.; Ratner, M. A. Interfering Pathways in Benzene: An Analytical Treatment. *J. Chem. Phys.* **2009**, *131*, 194704.